NUCLEAR SCIENCE AND ENGINEERING: **79**, 340-356 (1981)

Fokker-Planck Calculations Using Standard Discrete Ordinates Transport Codes

J. E. Morel

Sandia National Laboratories, Theoretical Division 4231, Albuquerque, New Mexico 87185

Received February 23, 1981
Accepted June 16, 1981

A method is developed for using standard discrete ordinates neutron transport codes to perform Fokker-Planck calculations in one-dimensional slab and spherical geometries. No modification of the codes is necessary and time-dependent, steady-state, forward, or adjoint calculations can be performed. It is shown that energy-angle integrated quantities such as energy and charge deposition profiles can be accurately and efficiently calculated for electrons. However, in certain types of problems, the number of groups required to converge the differential energy spectra can be prohibitively large.

INTRODUCTION

The purpose of this paper is to present a discrete ordinates method[1] for solving the Fokker-Planck equation. This equation represents an approximation to the Boltzmann transport equation that is valid whenever small-angle scattering is predominant.[2] By small-angle scattering we mean scattering resulting in both a small scattering angle and a small energy loss. The Fokker-Planck equation is most often used to describe the transport of energetic charged particles in plasmas. Interest in its solution has increased markedly in recent years primarily because of the importance of charged-particle transport phenomena in controlled-fusion schemes.[3-5]

Many methods have been developed to solve the Fokker-Planck equation, but most of them are limited in scope. For instance, the multigroup-diffusion method of Corman et al.[6] is not suitable for problems with localized or highly anisotropic sources. The moments technique of Haldy and Ligou[7] is limited to infinite-medium problems. The LSN method of Antal and Lee[8] and the integral tracking technique of Moses[9] account for energy losses due to scattering but ignore angular deflections.

One of the most general methods developed to date appears to be the S_n method of Mehlhorn and Duderstadt.[10] These authors modified the TIMEX code[11] to obtain the TIMEX-FP code,[10] which can provide time-dependent Fokker-Planck solutions in one-dimensional slab and spherical geometries. Our

[1]B. G. CARLSON, "The Numerical Theory of Neutron Transport," *Methods of Computational Physics*, Vol. 1, Statistical Physics, Academic Press, Inc., New York (1963).

[2]B. S. TANNENBAUM, *Plasma Physics*, McGraw-Hill Book Company, Inc., New York (1967).

[3]G. W. KUSWA, "Progress Towards Fusion with Light Ions," *Proc 8th Int. Conf. Plasma Physics and Controlled Nuclear Fusion Research*, Brussels, Belgium, July 1-10, 1980, IAEA-CN-381P3, International Atomic Energy Agency (1980).

[4]K. A. BRUCKNER and S. JORNA, *Rev. Mod. Phys.*, **46**, 325 (1974).

[5]L. A. ARTSIMOVICH, *Nucl. Fus.*, **12**, 215 (1972).

[6]E. G. CORMAN, W. E. LOEWE, G. E. COOPER, and A. M. WINSLOW, *Nucl. Fus.*, **15**, 377 (1975).

[7]P. A. HALDY and J. LIGOU, *Nucl. Fus.*, **17**, 1225 (1977).

[8]M. J. ANTAL and C. J. LEE, *J. Comp. Phys.*, **20**, 298 (1976).

[9]G. A. MOSES, *Nucl. Sci. Eng.*, **64**, 49 (1977).

[10]T. A. MEHLHORN and J. J. DUDERSTADT, *J. Comp. Phys.*, **38**, 86 (1980).

[11]T. R. HILL and W. H. REED, "TIMEX: A Time-Dependent Explicit Discrete Ordinates Program for the Solution of Multigroup Transport Equations with Delayed Neutrons," LA-6201-MS, Los Alamos National Laboratory (1976).

0029-5639/81/0012-0340$02.00/0

method differs from theirs in several respects, but the most important is that our method can be implemented in standard one-dimensional S_n codes (steady state or time dependent), such as TIMEX (Ref. 11), ONETRAN (Ref. 12), TDA (Ref. 13), and ANISN (Ref. 14), without modifying them. Appropriate multigroup Legendre cross-section expansions need simply be input. For reasons discussed later, our method is limited to slab and spherical geometries.

In this paper, we first derive the particular form of the Fokker-Planck equation that we solve. Then our numerical treatment of the Fokker-Planck equation is discussed. Computational results are presented, followed by conclusions and recommendations for future work.

THE FOKKER-PLANCK EQUATION

The Fokker-Planck equation can take many different forms depending on the order of approximation employed and the characteristics of the scattering cross section. In all cases, the integral Boltzmann scattering operator is approximated with a differential operator obtained using Taylor expansion techniques. In this section, we derive a well-known Fokker-Planck equation that is second-order accurate and appropriate for problems with the following characteristics:

1. one-dimensional slab or spherical geometry
2. an isotropic transport medium
3. forward-peaked elastic scattering.

The derivation begins with the Boltzmann equation, which, in one-dimensional slab and spherical geometries, can be expressed as[15]

$$\nabla\cdot\Omega\psi(r,\mu,E)+\sigma_t(r,E)\psi(r,\mu,E) = \int_0^{\infty}\int_0^{2\pi}\int_{-1}^{+1}\sigma_s(r,E'\to E,\mu_0)\psi(r,\mu',E')d\mu'd\phi'dE' + Q(r,\mu,E) \ , \quad (1a)$$

where

$$\mu_0=\mu'\mu+[(1-\mu^2)(1-\mu^2)]^{1/2}\cos(\phi') \ . \quad (1b)$$

For the sake of simplicity in the expressions that follow, we suppress much of the variable notation. The dependencies exhibited by the various quantities appearing in Eq. (1a) henceforth apply to these and similar quantities unless otherwise stated. With elastic scattering, the energy loss and scattering angle are coupled and the differential scattering cross section can be expressed in either of two ways:

$$\sigma_s(E'\to E,\mu_0)=\sigma_s(E',\mu_0)\,\delta(E-E_s) \quad (2a)$$

with

$$E_s=E_s(E',\mu_0) \ , \quad (2b)$$

or

$$\sigma_s(E'\to E,\mu_0)=\sigma_s(E'\to E)\,\delta(\mu_0-\mu_s) \quad (2c)$$

with

$$\mu_s=\mu_s(E',E) \ . \quad (2d)$$

When $\mu_0 = 1$, $E_s = E'$ and when $E' = E$, $\mu_s = 1$. Substitution of Eq. (2a) into Eq. (1a) with some manipulation gives

$$\nabla\cdot\Omega\psi+\sigma_a\psi=\Gamma_B\psi+Q \ , \quad (3a)$$

where

$$\Gamma_B\psi=\int_0^{2\pi}\int_{-1}^{+1}[\sigma_s(E',\mu_0)\psi(\mu',E') - \sigma_s(E,\mu_0)\psi(\mu,E)]d\mu'd\phi' \ , \quad (3b)$$

and E' is a function of E and μ_0 such that

$$E=E_s(E',\mu_0) \ . \quad (3c)$$

We refer to Γ_B as the Boltzmann scattering operator. It is this integral operator that is replaced with an approximate differential operator to obtain the Fokker-Planck equation.

In order to proceed, it is necessary to change the integration variables in Eq. (3b). Let θ_0 and ϕ_0 be defined with respect to a coordinate system aligned along the direction Ω as shown in Figs. (1a) and (1b). Changing to these variables gives

$$\Gamma_B\psi=\int_0^{2\pi}\int_{-1}^{+1}[\sigma_s(E',\mu_0)\psi(\mu',E) - \sigma_s(E,\mu_0)\psi(\mu,E)]\sin\theta_0 d\theta_0 d\phi_0 \ , \quad (4a)$$

where

$$\mu_0=\cos\theta_0 \ , \quad (4b)$$

and

$$\mu'=\mu\cos\theta_0-(1-\mu^2)^{1/2}\sin\theta_0\cos\phi_0 \ . \quad (4c)$$

---

[12]T. R. HILL, "ONETRAN: A Discrete Ordinates Finite Element Code for the Solution of the One-Dimensional Multigroup Transport Equation," LA-5990-MS, Los Alamos National Laboratory (1975).

[13]S. A. DUPREE, H. A. SANDMEIER, G. E. HANSEN, W. W. ENGLE, Jr., and F. R. MYNATT, "Time-Dependent Neutron and Photon Transport Calculations Using the Method of Discrete Ordinates," LA-4557, Los Alamos National Laboratory (1971).

[14]W. W. ENGLE, Jr., "A User's Manual for ANISN," K-1693, Union Carbide Corporation Nuclear Division, Oak Ridge, Tennessee (1967).

[15]G. I. BELL and S. GLASSTONE, *Nuclear Reactor Theory*, Van Nostrand Reinhold Co., New York (1970).

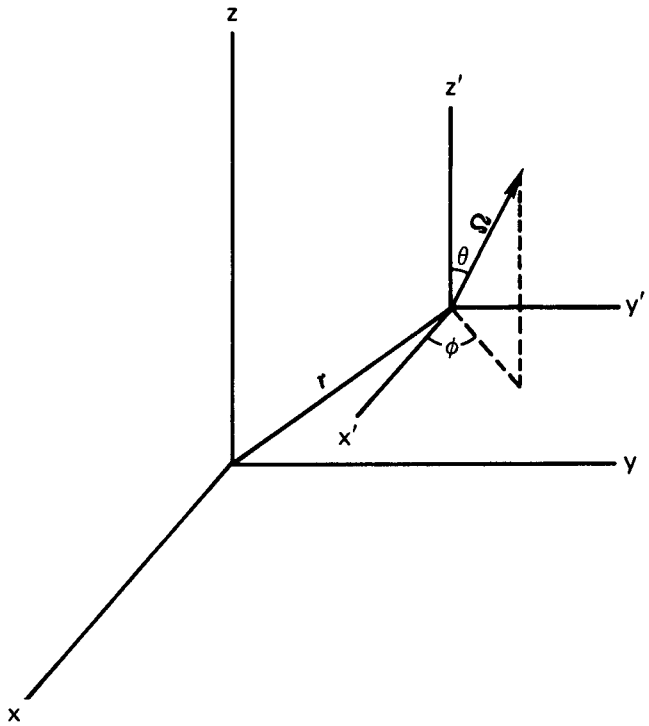

Fig. 1a. Standard phase-space coordinate system.

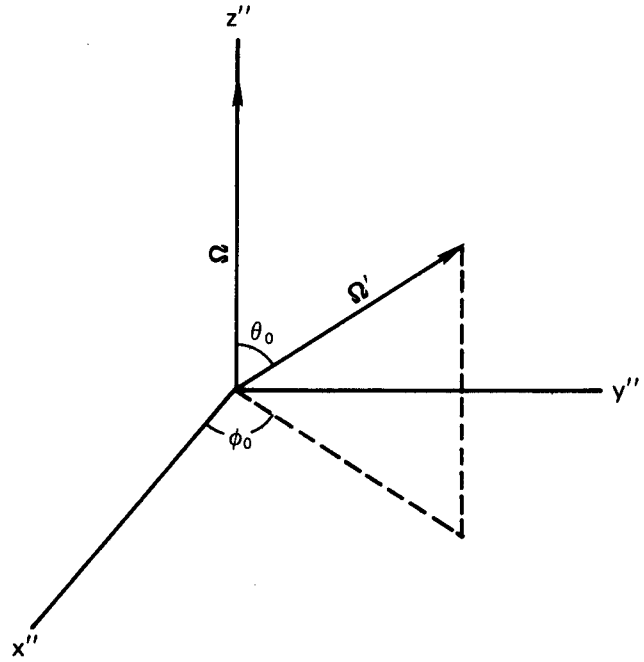

Fig. 1b. Direction-space coordinate system aligned along $\boldsymbol{\Omega}$. The (x'',y'',z'') axes are obtained from the (x',y',z') axes shown in Fig. 1a by first rotating about the z' axes through an angle equal to ϕ to fix the y'' axis, and then rotating about the y'' axis through an angle equal to θ to fix the x'' and z'' axes.

Performing a Taylor series expansion about $\theta_0 = 0$ and retaining terms up to θ_0^2 gives

$$\sigma_s(E',\mu_0)\psi(\mu',E) - \sigma_s(E,\mu_0)\psi(\mu,E) = I_1 + I_2 \ , \quad (5a)$$

where

$$I_1 = \sigma_s(E,\mu_0)\left[\frac{\partial}{\partial\mu}\psi(\mu,E)\left(\frac{\partial\mu'}{\partial\theta_0}\theta_0 + \frac{1}{2}\frac{\partial^2\mu'}{\partial\theta_0^2}\theta_0^2\right) + \frac{1}{2}\frac{\partial^2}{\partial\mu^2}\psi(\mu,E)\left(\frac{\partial\mu'}{\partial\theta_0}\right)^2\theta_0^2\right] \quad (5b)$$

and

$$I_2 = \frac{\partial}{\partial E}\sigma_s(E,\mu_0)\psi(\mu,E)\left(\frac{\partial E'}{\partial\theta_0}\theta_0 + \frac{1}{2}\frac{\partial^2 E'}{\partial\theta_0^2}\theta_0^2\right) + \frac{1}{2}\frac{\partial^2}{\partial E^2}\sigma_s(E,\mu_0)\psi(\mu,E)\left(\frac{\partial E'}{\partial\theta_0}\right)^2\theta_0^2 \ . \quad (5c)$$

Using Eq. (4c) to evaluate the derivatives in Eq. (5b) gives

$$I_1 = \sigma_s(E,\mu_0)\theta_0^2\left[-\frac{\mu}{2}\frac{\partial\psi}{\partial\mu} + \frac{(1-\mu^2)}{2}(\cos\phi_0)^2\frac{\partial^2\psi}{\partial\mu^2}\right] . \quad (6)$$

Because $E = E_s(E',\theta_0)$ and $E' = E$ when $\theta_0 = 0$, it follows that

$$\frac{\partial E'}{\partial\theta_0}\theta_0 + \frac{1}{2}\frac{\partial^2 E'}{\partial\theta_0^2}\theta_0^2 + \ldots = -\frac{\partial E_s}{\partial\theta_0}\theta_0 - \frac{1}{2}\frac{\partial E_s}{\partial\theta_0^2}\theta_0^2 + \ldots = E - E_s(E,\theta_0) \ . \quad (7)$$

Taking this into account, Eq. (5c) becomes

$$I_2 = \frac{\partial}{\partial E}\sigma_s(E,\mu_0)\psi(\mu,E)(E-E_s) + \frac{1}{2}\frac{\partial^2}{\partial E^2}\sigma_s(E,\mu_0)\psi(\mu,E)(E-E_s)^2 \ . \quad (8)$$

Substituting Eqs. (6) and (8) into Eq. (4a) and integrating gives

$$\Gamma_B\psi \approx \Gamma_{FP}\psi \quad (9a)$$

where

$$\Gamma_{FP}\psi = \frac{\alpha}{2}\frac{\partial}{\partial\mu}(1-\mu^2)\frac{\partial}{\partial\mu}\psi + \frac{\partial}{\partial E}\beta\psi + \frac{1}{2}\frac{\partial^2}{\partial E^2}\gamma\psi \quad (9b)$$

and

$$\alpha = 2\pi\int_{-1}^{+1}\sigma_s(E,\mu_0)(1-\mu_0)d\mu_0 \ , \quad (9c)$$

$$\beta = \int_0^\infty \sigma_s(E\to E')(E-E')dE' \ , \quad (9d)$$

$$\gamma = \int_0^\infty \sigma_s(E\to E')(E-E')^2dE' \ . \quad (9e)$$

We refer to Γ_{FP} as the Fokker-Planck scattering operator. The functions α, β, and γ are known as

the momentum transfer, stopping power,[16] and mean-square stopping power, respectively. We refer to them collectively as the Fokker-Planck functions. Substitution of Γ_{FP} for Γ_B in Eq. (3a) yields the Fokker-Planck equation that we seek to solve:

$$\nabla\cdot\Omega\psi + \sigma_a\psi = \Gamma_{FP}\psi + Q \ . \tag{10}$$

If the angular flux is sufficiently smooth, the expansions given in Eqs. (5b) and (5c) are accurate for "small" values of θ_0. If the scattering is highly forward peaked, the integrand in Eq. (4a) is significantly nonzero over only a "small" region about $\theta_0 = 0$. Thus, one would expect that with sufficiently forward-peaked scattering, the dominant contribution to the Boltzmann integral would come from the range of θ_0 values over which the expansions are accurate and that $\Gamma_{FP}\psi$ would thereby closely approximate $\Gamma_B\psi$. This is sometimes the case, but in many problems difficulties arise because the angular flux derivatives with respect to energy are either unbounded or extremely large. Thus, it is usually difficult to make an *a priori* estimate of the accuracy of the Fokker-Planck equation based on theoretical results. Experience has shown that good results for scalar quantities (angle and energy integrated), such as energy and charge deposition profiles, can be expected in charged-particle calculations. However, results for detailed differential quantities are generally inadequate. The Fokker-Planck equation is very useful in spite of this deficiency because it is the scalar rather than differential quantities that are most often of applied interest.

NUMERICAL TREATMENT OF THE FOKKER-PLANCK EQUATION

In the previous section, it was shown that the Fokker-Planck equation approximates the Boltzmann equation when the scattering is highly forward-peaked. It therefore follows that the Boltzmann equation must approximate the Fokker-Planck equation under similar conditions. This would seem to be a rather trivial conclusion, but it suggests the indirect approach that we employ to solve the Fokker-Planck equation. The central idea of our method is to define multigroup Legendre cross-section expansion coefficients in terms of the Fokker-Planck functions and certain S_n parameters so that the Boltzmann solutions corresponding to these coefficients converge to the desired Fokker-Planck solution as the S_n space-angle-energy mesh is refined. The S_n parameters on which the coefficients depend are the order of the quadrature set and the energy group structure. For reasons explained later, our method requires that Gauss quadrature sets be used and, further, that Legendre expansions of degree $(N - 1)$ be used in conjunction with quadrature sets of order N. Further analysis of the Fokker-Planck equation is necessary to explain our technique.

The Fokker-Planck equation was derived under the assumption of an elastic-scattering cross section of the form given in Eq. (2a). It is important to note, however, that all information on the angle-energy coupling of the scattering is lost in the Fokker-Planck approximation. For instance, defining

$$\Gamma^{\alpha}_{FP}\psi = \frac{\alpha}{2}\frac{\partial}{\partial\mu}(1-\mu^2)\frac{\partial}{\partial\mu}\psi \tag{11a}$$

and

$$\Gamma^{e}_{FP}\psi = \frac{\partial}{\partial E}\beta\psi + \frac{1}{2}\frac{\partial^2}{\partial E^2}\gamma\psi \ , \tag{11b}$$

we note that Γ^{α}_{FP} causes particles to redistribute in direction without energy change, while Γ^{e}_{FP} causes particles to redistribute in energy without directional change. This would suggest that Γ^{α}_{FP} should be approximated with a cross section of the form

$$\sigma_s(E'\to E,\mu_0) = \sigma^{\alpha}(E,\mu_0)\delta(E'-E) \ , \tag{12a}$$

while Γ^{e}_{FP} should be approximated by a cross section of the form

$$\sigma_s(E'\to E,\mu_0) = \sigma^{e}(E'\to E)\frac{1}{2\pi}\delta(\mu_0 - 1) \ . \tag{12b}$$

Additional justification for this decoupled approximation is found in the fact that the Fokker-Planck scattering operator given in Eq. (9b) can also be derived assuming a composite decoupled cross section:

$$\sigma_s(E'\to E,\mu_0) = \sigma^{\alpha}(E,\mu_0)\delta(E'-E) + \sigma^{e}(E'\to E)\frac{1}{2\pi}\delta(\mu_0 - 1) \ . \tag{13}$$

As one would expect, the derivation is very similar to that for the elastic (coupled) cross section. Hence, we only give a brief outline of it.

The Boltzmann scattering operators corresponding to σ^{α} and σ^{e} are

$$\Gamma^{\alpha}_{B} = \int_0^{2\pi}\int_{-1}^{+1}\sigma^{\alpha}(E,\mu_0)[\psi(\mu') - \psi(\mu)]d\mu' d\phi' \tag{14a}$$

and

$$\Gamma^{e}_{B} = \int_0^{\infty}[\sigma^{e}(E'\to E)\psi(E') - \sigma^{e}(E\to E')\psi(E)]dE' \ , \tag{14b}$$

respectively. Expanding the integrand in Eq. (14a) about $\theta_0 = 0$, where θ_0 is as given in Eq. (4b), keeping terms up to θ_0^2, and integrating gives

$$\Gamma^{\alpha}_{B} = \Gamma^{\alpha}_{FP}\psi \ , \tag{15a}$$

[16]The stopping power as we have defined it is positive when particles lose energy on the average. It is often defined with the opposite sign convention.

with

$$\alpha = 2\pi \int_{-1}^{+1} \sigma^{\alpha}(E,\mu_0)(1-\mu_0)d\mu_0 \ . \qquad (15b)$$

Expanding the integrand in Eq. (14b) about $\tau = 0$, where $\tau = E' - E$, keeping terms up to τ^2, and integrating gives

$$\Gamma_B^e \psi = \Gamma_{FP}^e \psi \qquad (16a)$$

with

$$\beta = \int_0^{\infty} \sigma^e(E \to E')(E - E')dE' \ , \qquad (16b)$$

$$\gamma = \int_0^{\infty} \sigma^e(E \to E')(E - E')^2 dE' \ . \qquad (16c)$$

An argument, completely analogous to that presented for the coupled case, can be used to show that Γ_B^{α} and Γ_{FP}^{α} better approximate one another as σ^{α} becomes increasingly peaked about $\mu_0 = 1$. For similar reasons, Γ_B^e and Γ_{FP}^e better approximate one another as σ^e becomes increasingly peaked about $E' = E$. Having established the properties that approximating cross sections should have, we now proceed to develop the desired multigroup Legendre expansion coefficients.

Coefficients for σ^{α}

Because σ^{α} does not change particle energy, it corresponds to a within-group cross section. Thus we need only define the Legendre coefficients, $\{\sigma_l^{\alpha}\}_{l=0}^{N-1}$. This is fairly straightforward to do once two fundamental properties of Γ_B^{α} and Γ_{FP}^{α} are noted. Let $\{P_l(\mu)\}_{l=0}^{\infty}$ denote the Legendre polynomials. By expanding σ^{α} in such polynomials and invoking the addition theorem for the spherical harmonics,[15] the following well-known result can be demonstrated:

$$\Gamma_B^{\alpha} P_l(\mu) = (\sigma_l^{\alpha} - \sigma_0^{\alpha}) P_l(\mu_0) \ , \quad l = 0, \infty \ , \qquad (17a)$$

where

$$\sigma_l^{\alpha} = 2\pi \int_{-1}^{+1} \sigma^{\alpha}(E,\mu_0) P_l(\mu_0) d\mu_0 \ . \qquad (17b)$$

Using standard recurrence relations for the Legendre polynomials,[15] it is not difficult to show that

$$\Gamma_{FP}^{\alpha} P_l(\mu) = \frac{\alpha}{2} l(l+1) P_l(\mu) \ , \quad l = 0, \infty \ . \qquad (18)$$

If the angular flux is expressible as a polynomial of arbitrary degree L,

$$\Psi(\mu) = \sum_{l=0}^{L} \frac{2l+1}{4\pi} \phi_l P_l(\mu) \ , \qquad (19)$$

then it follows from Eqs. (17a) and (18) that we can define σ^{α} so that

$$\Gamma_B^{\alpha} \psi = \Gamma_{FP}^{\alpha} \psi \qquad (20)$$

by setting

$$\sigma_0^{\alpha} - \sigma_l^{\alpha} = \frac{\alpha}{2} l(l+1) \ , \quad l = 1, L \ . \qquad (21)$$

Choosing $\sigma_L = 0$ so as to minimize the resulting value for σ_0^{α}, Eq. (21) gives

$$\sigma^{\alpha}(E,\mu_0) = \sum_{l=0}^{L} \frac{2l+1}{4\pi} \sigma_l^{\alpha} P_l(\mu_0) \ , \qquad (22a)$$

where

$$\sigma_l^{\alpha} = \frac{\alpha}{2} [L(L+1) - l(l+1)] \ , \quad l = 0, L \ . \qquad (22b)$$

Thus, with an expansion degree of L for σ^{α}, we see that Γ_B^{α} and Γ_{FP}^{α} are completely equivalent when operating on polynomials of degree L or less. We now demonstrate that it is particularly advantageous to use an expansion of degree $(N-1)$ in conjunction with a Gauss quadrature set of order N.

Let $\{\psi_i\}_{i=1}^N$ be the discrete angular flux values defined at the Gauss quadrature points, $\{\mu_i\}_{i=1}^N$, having associated weights, $\{w_i\}_{i=1}^N$. The discrete ordinates approximation for the discrete values of $\Gamma_B^{\alpha}\psi$ is

$$\sum_{l=0}^{N-1} \frac{2l+1}{4\pi} \sigma_l \left[\sum_{k=1}^{N} \psi_k P_l(\mu_k) w_k \right] P_l(\mu_i) - \sigma_0^{\alpha} \psi_i \ , \quad i = 1, N \ . \qquad (23)$$

Let $\psi_p(\mu)$ be the unique polynomial of degree $(N-1)$ or less, which interpolates the discrete angular flux values. Applying Γ_{FP}^{α} to $\psi_p(\mu)$ gives

$$\Gamma_{FP}^{\alpha} \psi_p(\mu) = \Gamma_B^{\alpha} \psi_p(\mu) = \sum_{l=0}^{N-1} \frac{2l+1}{4\pi} \sigma_l^{\alpha} \phi_l P_l(\mu) - \sigma_0 \psi_p(\mu) \ , \qquad (24a)$$

where

$$\phi_l = 2\pi \int_{-1}^{+1} \psi_p(\mu) P_l(\mu) d\mu \ , \quad l = 0 \ , \quad N-1 \ . \qquad (24b)$$

Because the integrand in Eq. (24b) is a polynomial of degree $(2N-1)$ or less, the integral can be evaluated exactly using the Gauss quadrature formula:

$$\phi_l = \sum_{k=1}^{N} \psi_k P_l(\mu_k) w_k \ . \qquad (25)$$

Substituting Eq. (25) into Eq. (24a) gives

$$\Gamma_{FP}^{\alpha} \psi_p(\mu) = \sum_{l=0}^{N-1} \frac{2l+1}{4\pi} \sigma_l^{\alpha} \left[\sum_{k=1}^{N} \psi_k P_l(\mu_k) w_k \right] \times P_l(\mu) - \sigma_0 \psi_p(\mu) \ . \qquad (26)$$

If Eq. (26) is successively evaluated at the quadrature points, Eq. (23) is obtained. Thus, we see that

with appropriate quadrature sets and expansion orders, the S_n representation for Γ^{α}_{FP} is equivalent to that obtained by interpolating the discrete angular flux values with a polynomial and operating on that polynomial with Γ^{α}_{FP}. It is well known[15] that one-dimensional slab geometry S_n calculations with Gauss quadrature sets and Legendre expansions of degree $(N-1)$ are equivalent to spherical-harmonics solutions of order $(N-1)$ with Mark boundary conditions. Assuming an expansion degree of $(N-1)$ for σ^{α}, the spherical-harmonics solution of order $(N-1)$ for the Boltzmann equation given by

$$\nabla\cdot\Omega\psi + \sigma_a\psi = \Gamma^{\alpha}_{B}\psi + Q \tag{27a}$$

must be identical to the spherical-harmonics solution of order $(N-1)$ for the Fokker-Planck equation given by

$$\nabla\cdot\Omega\psi + \sigma_a\psi = \Gamma^{\alpha}_{FP}\psi + Q \ , \tag{27b}$$

because Γ^{α}_{B} and Γ^{α}_{FP} are equivalent when operating on polynomials of degree $(N-1)$ or less. Taking the established equivalence between S_n and spherical-harmonics solutions into account, it follows that one-dimensional slab geometry S_n solutions for Eq. (27a) obtained using Gauss quadrature sets of order N in conjunction with σ^{α} expansions of degree $(N-1)$ must be equivalent to the spherical-harmonics solution of order $(N-1)$ with Mark boundary conditions for Eq. (27b). This is clearly an important and highly desirable characteristic of our S_n treatment for the Γ^{α}_{FP} operator.

It is instructive to consider the behavior of σ^{α} in the limit as the degree of the expansion is increased. Previous analysis shows that σ^{α} better approximates Γ^{α}_{B} as it becomes increasingly forward-peaked. In addition, it should obviously have the correct momentum transfer. Thus, we first take note that regardless of expansion order the momentum transfer of σ^{α} is exact:

$$\begin{aligned} 2\pi\int_{-1}^{+1}\sigma^{\alpha}(E,\mu_0)(1-\mu_0)d\mu_0 &= \sigma_0-\sigma_1 \\ &= \frac{\alpha}{2}L(L+1)-\frac{\alpha}{2}[L(L+1)-2] \\ &= \alpha \ . \end{aligned} \tag{28}$$

The average cosine of the scattering angle can be expressed as follows:

$$\begin{aligned} \bar{\mu}_0 &= \sigma^{\alpha}_1/\sigma^{\alpha}_0 \ , \\ &= \frac{L(L+1)-2}{L(L+1)} \ . \end{aligned} \tag{29}$$

It is easily seen that as L increased, $\bar{\mu}_0$ goes to unity. Thus, σ^{α} becomes increasingly forward-peaked as L increases. The total magnitude of σ^{α} becomes unbounded in the same limit:

$$\sigma^{\alpha}_0 = \frac{\alpha}{2}L(L+1) \ . \tag{30}$$

Expressing the momentum transfer as follows:

$$\alpha = \sigma^{\alpha}_0(1-\bar{\mu}_0) \ , \tag{31}$$

it is seen that σ^{α}_0 must increase without bound if the momentum transfer is to remain constant as σ^{α} becomes increasingly forward-peaked. This shows that Γ^{α}_{FP} corresponds to a type of continuous-deflection approximation. The Γ^{α}_{FP} operator effectively causes particles to scatter continuously while incurring a differential deflection in each scattering event. The net result is that particles continuously deflect with the mean deflection per unit pathlength given by the momentum transfer.

In concluding our discussion of σ^{α}, we point out that the expansion of σ^{α} for any finite value of L must be viewed as a truncated expansion for a singular cross section. Upon examination we have found that σ^{α} is always negative over certain regions if the expansion order is greater than unity. Our computational results indicate that these negative oscillations do not adversely affect angle-integrated quantities, but they do cause the angular flux to occasionally become negative along certain directions. Because the Fokker-Planck equation is generally useful only for calculating angle- and energy-integrated quantities, we feel that this shortcoming is acceptable.

Coefficients for σ^{e}

Because σ^{e} causes particles to redistribute only in energy, we need only define group-to-group transfer cross sections. It is seen from Eq. (12b) that a truncated Legendre expansion for $\delta(\mu_0-1)$ must be used in conjunction with these transfer cross sections. The validity of such an expansion is obviously questionable. After defining and analyzing the transfer cross sections, we show that with the proper choice of quadrature sets and associated Legendre expansion degrees, the truncated delta-function expansion can be made to operate on the discrete angular flux values in an exact manner.

It is convenient for our purposes to decompose σ^{e} into a sum of two cross sections:

$$\sigma^{e}(E'\to E) = \sigma^{\beta}(E'\to E) + \sigma^{\gamma}(E'\to E) \ . \tag{32}$$

As the notation suggests, σ^{β} and σ^{γ} are intended to approximate the operators containing β and γ, Γ^{β}_{FP} and Γ^{γ}_{FP}, respectively. We first define and analyze continuous (as opposed to multigroup) representations for σ^{β} and σ^{γ}. The information obtained in the analysis is then used to construct the multigroup transfer cross sections. Consider the following continuous definitions for the cross sections:

$$\sigma^{\beta}(E' \to E) = \frac{2\beta(E')}{\Delta E^2} \ , \quad \text{for } 0 \leqslant E' - E \leqslant \Delta E \text{ if } \beta(E') \geqslant 0 \ ,$$

$$= \frac{2\beta(E')}{\Delta E^2} \ , \quad \text{for } -\Delta E \leqslant E' - E \leqslant 0 \text{ if } \beta(E') < 0 \ ,$$

$$= 0 \ , \quad \text{otherwise} \tag{33}$$

$$\sigma^{\gamma}(E' \to E) = \frac{3\gamma(E')}{2\Delta E^3} \ , \quad \text{for } -\Delta E \leqslant E' - E \leqslant \Delta E \ ,$$

$$= 0 \ , \quad \text{otherwise} \ . \tag{34}$$

For the sake of simplicity, we consider only the $\beta(E') \geqslant 0$ case in the following analysis.

The scalar magnitude, stopping power, and mean-square stopping power of σ^{β} are

$$\int_{E-\Delta E}^{E} \frac{2\beta(E)}{\Delta E^2} dE' = \frac{2\beta(E)}{\Delta E} \ , \tag{35a}$$

$$\int_{E-\Delta E}^{E} \frac{2\beta(E)}{\Delta E^2} (E - E') dE' = \beta(E) \ , \tag{35b}$$

and

$$\int_{E-\Delta E}^{E} \frac{2\beta(E)}{\Delta E^2} (E - E')^2 dE' = \frac{2}{3} \beta(E) \Delta E \ , \tag{35c}$$

respectively. These same quantities are given for σ^{γ} by

$$\int_{E-\Delta E}^{E+\Delta E} \frac{3\gamma(E)}{2\Delta E^3} dE' = \frac{3\gamma(E)}{2\Delta E^2} \ , \tag{36a}$$

$$\int_{E-\Delta E}^{E+\Delta E} \frac{3\gamma(E)}{2\Delta E^3} (E - E') dE' = 0 \ , \tag{36b}$$

and

$$\int_{E-\Delta E}^{E+\Delta E} \frac{3\gamma(E)}{2\Delta E^2} (E - E')^2 dE' = \gamma(E) \ . \tag{36c}$$

Thus, the scalar magnitude, stopping power, and mean-square stopping power of σ^{e} are

$$\int_{E-\Delta E}^{E+\Delta E} \sigma^{e}(E \to E') dE' = \frac{2\beta(E)}{\Delta E} + \frac{3\gamma(E)}{2\Delta E^2} \ , \tag{37a}$$

$$\int_{E-\Delta E}^{E+\Delta E} \sigma^{e}(E \to E')(E - E') dE' = \beta(E) \ , \tag{37b}$$

and

$$\int_{E-\Delta E}^{E+\Delta E} \sigma^{e}(E \to E')(E - E')^2 dE' = \gamma(E) + \frac{2}{3} \beta(E) \Delta E \ , \tag{37c}$$

respectively. It is clear that as ΔE goes to zero, σ^{e} becomes increasingly peaked about $E' = E$. Although it always has the correct stopping power, σ^{e} attains the correct mean-square stopping power only in the limit of decreasing ΔE. The Boltzmann operators corresponding to σ^{β} and σ^{γ} are

$$\Gamma_{B}^{\beta}\psi = \int_{E}^{E+\Delta E} \left[\frac{2\beta(E')}{\Delta E^2} \psi(E') - \frac{2\beta(E)}{\Delta E^2} \psi(E) \right] dE' \ , \tag{38}$$

and

$$\Gamma_{B}^{\gamma}\psi = \int_{E}^{E+\Delta E} \left[\frac{3\gamma(E')}{2\Delta E^3} \psi(E') - \frac{3\gamma(E)}{2\Delta E^3} \psi(E) \right] dE' \ . \tag{39}$$

Expanding each integrand in a Taylor series about $E' = E$ and integrating gives

$$\Gamma_{B}^{\beta}\psi = \frac{\partial}{\partial E} \beta\psi + \frac{\partial^2}{\partial E^2} \beta\psi \left(\frac{\Delta E}{3} \right) + \frac{\partial^3}{\partial E^3} \beta\psi \left(\frac{\Delta E^2}{12} \right) + \ldots \ , \tag{40}$$

and

$$\Gamma_{B}^{\gamma}\psi = \frac{1}{2} \frac{\partial^2}{\partial E^2} \gamma\psi + \frac{\partial^4}{\partial E^4} \gamma\psi \left(\frac{\Delta E^2}{40} \right) + \frac{\partial^6}{\partial E^6} \gamma\psi \left(\frac{\Delta E^4}{1680} \right) + \ldots \ . \tag{41}$$

It is clear from Eqs. (40) and (41) that as ΔE decreases, Γ_{B}^{β} and Γ_{B}^{γ} become equivalent to Γ_{FP}^{β} and Γ_{FP}^{γ}, respectively.

By observing the behavior of σ^{β} and σ^{γ} in the limit as ΔE goes to zero, we can gain insight into the characteristics of Γ_{FP}^{β} and Γ_{FP}^{γ}. As ΔE decreases, the scalar magnitudes of σ^{β} and σ^{γ} become unbounded. This means that both Γ_{FP}^{β} and Γ_{FP}^{γ} correspond to a type of continuous scattering approximation. The effect of each operator, however, is quite different. It is well known that the use of Γ_{FP}^{β} alone corresponds to the continuous slowing down approximation.[17] This operator causes particles to lose energy continuously with the energy loss per unit pathlength given by the stopping power. Conversely, the stopping power of σ^{γ} is zero. Every collision in which a particle loses energy is balanced by one in which a particle gains energy. Thus, Γ_{FP}^{γ} causes particles to "diffuse" in energy space. This introduces energy-loss straggling into the calculation. The mean-square energy change incurred per unit pathlength is given by the mean-square stopping power.

Having defined a continuous version of σ^{e}, one might be tempted to choose a value for ΔE based on the energy group structure (in much the same way that the expansion degree for σ^{α} is chosen based on the quadrature order) and simply generate standard multigroup transfer coefficients corresponding to σ^{e}.

[17] ROBLEY D. EVANS, *The Atomic Nucleus*, McGraw-Hill Book Company, New York (1955).

However, we have found this approach to be generally unacceptable. The reason for this is that the multigroup method is designed to conserve particle number, but not necessarily energy. As a result, the stopping power and mean-square stopping power for σ^e calculated in a manner consistent with the multigroup approximation are generally not equal to the values given in Eqs. (37b) and (37c). We therefore define multigroup coefficients for σ^e that are based entirely on energy rather than particle conservation requirements.

For instance, let $\sigma_{g\to k}$ denote the probability per unit pathlength that a particle will scatter without angular redistribution from group g to group k. Further, let $E_{g-1/2}$, E_g, and $E_{g+1/2}$ denote the upper endpoint, midpoint, and lower endpoint energies, respectively, for group g. The multigroup cross sections corresponding to σ^β and σ^γ are defined as follows:

$$\sigma^\beta_{g\to k} = \frac{\beta(E_g)}{E_g - E_k} \quad \begin{matrix} \text{for } k = g+1, \text{ if } \beta(E_g) \geqslant 0 \text{ , and} \\ \text{for } k = g-1, \text{ if } \beta(E_g) < 0 \text{ ,} \end{matrix}$$
$$= 0 \text{ , for all other values of } k \tag{42}$$

and

$$\sigma^\gamma_{g\to k} = \frac{\gamma(E_g)}{2(E_g - E_k)^2} \text{ , for } k = g-1 \text{ and } k = g+1$$
$$= 0 \text{ , for all other values of } k \text{ .} \tag{43}$$

The construction of these multigroup cross sections is clearly analogous to that of the continuous ones. Again, for simplicity, we analyze only the $\beta(E_g) \geqslant 0$ case.

The scalar magnitude, stopping power, and mean-square stopping power of a multigroup cross section can be calculated using the following respective expressions:

$$\sigma_g = \sum_{k=1}^{NG} \sigma_{g\to k} \text{ ,} \tag{44a}$$

$$\beta_g = \sum_{k=1}^{NG} \sigma_{g\to k}(E_g - E_k) \text{ ,} \tag{44b}$$

and

$$\gamma_g = \sum_{k=1}^{NG} \sigma_{g\to k}(E_g - E_k)^2 \text{ ,} \tag{44c}$$

where NG denotes the total number of groups. Applying these equations to σ^β and σ^γ gives

$$\sum_{k=1}^{NG} \sigma^\beta_{g\to k} = \frac{\beta(E_g)}{E_g - E_{g+1}} \text{ ,} \tag{45a}$$

$$\sum_{k=1}^{NG} \sigma^\beta_{g\to k}(E_g - E_k) = \beta(E_g) \text{ ,} \tag{45b}$$

$$\sum_{k=1}^{NG} \sigma^\beta_{g\to k}(E_g - E_k)^2 = \beta(E_g)(E_g - E_{g+1}) \text{ ,} \tag{45c}$$

and

$$\sum_{k=1}^{NG} \sigma^\gamma_{g\to k} = \frac{\gamma(E_g)}{2(E_g - E_{g-1})^2} + \frac{\gamma(E_g)}{2(E_g - E_{g+1})^2} \text{ ,} \tag{46a}$$

$$\sum_{k=1}^{NG} \sigma^\gamma_{g\to k}(E_g - E_k) = 0 \text{ ,} \tag{46b}$$

$$\sum_{k=1}^{NG} \sigma^\gamma_{g\to k}(E_g - E_k)^2 = \gamma(E_g) \text{ .} \tag{46c}$$

The scalar magnitude, stopping power, and mean-square stopping power for σ_e are, therefore,

$$\sum_k \sigma^e_{g\to k} = \frac{\beta(E_g)}{E_g - E_{g+1}} + \frac{\gamma(E_g)}{2(E_g - E_{g-1})^2} + \frac{\gamma(E_g)}{2(E_g - E_{g+1})^2} \text{ ,} \tag{47a}$$

$$\sum_k \sigma^e_{g\to k}(E_g - E_k) = \beta(E_g) \text{ ,} \tag{47b}$$

and

$$\sum_k \sigma^e_{g\to k}(E_g - E_k)^2 = \gamma(E_g) + \beta(E_g)(E_g - E_{g+1}) \text{ ,} \tag{47c}$$

respectively. Analogous to the continuous version of σ^e, the multigroup version always has the correct stopping power, but the correct mean-square stopping power is only attained in the limit as the maximum group width goes to zero.

It is interesting to note that with a certain type of group structure, our multigroup treatment for Γ^β_{FP} and Γ^γ_{FP} becomes equivalent to a standard finite difference treatment. For instance, consider the following simplified Fokker-Planck equation:

$$\nabla\cdot\bar{\Omega}\psi = \frac{\partial}{\partial E}\beta\psi + \frac{1}{2}\frac{\partial^2}{\partial E^2}\gamma\psi \text{ .} \tag{48}$$

Denoting the angular flux for group g by ψ_g and applying our multigroup representations for Γ^β_{FP} and Γ^γ_{FP}, Eq. (48) becomes

$$\nabla\cdot\bar{\Omega}\psi_g + (\sigma^\beta_{g\to g+1} + \sigma^\gamma_{g\to g-1} + \sigma^\gamma_{g\to g+1})\psi_g = (\sigma^\beta_{g-1\to g} + \sigma^\gamma_{g-1\to g})\psi_{g-1} + \sigma^\gamma_{g+1\to g}\psi_{g+1} \text{ .} \tag{49}$$

If we assume a *uniform* energy group width ΔE and substitute from Eqs. (42) and (43) into Eq. (49), we obtain

$$\nabla\cdot\Omega\psi_g + \left[\frac{\beta(E_g)}{\Delta E} + \frac{\gamma(E_g)}{2\Delta E^2} + \frac{\gamma(E_g)}{2\Delta E^2}\right]\psi_g = \left[\frac{\beta(E_{g-1})}{\Delta E} + \frac{\gamma(E_{g-1})}{2\Delta E^2}\right]\psi_{g-1} + \frac{\gamma(E_{g+1})}{2\Delta E^2}\psi_{g-1} \ . \quad (50)$$

Rearranging terms and assuming that the midpoint differential angular flux value $\psi(E_g)$ is related to the multigroup value by $\psi(E_g)\Delta E = \psi_g$, we get

$$\nabla\cdot\Omega\psi(E_g) = \frac{\beta(E_{g-1})\psi(E_{g-1}) - \beta(E_g)\psi(E_g)}{\Delta E} + \frac{1}{2}\frac{\gamma(E_{g-1})\psi(E_{g-1}) - 2\gamma(E_g)\psi(E_g) + \gamma(E_{g+1})\psi(E_{g+1})}{\Delta E^2} \ . \quad (51)$$

Thus, it is seen that with a uniform energy group width, our treatment for Γ^{β}_{FP} is equivalent to a standard first-order backward-difference approximation, while our treatment for Γ^{γ}_{FP} is equivalent to a standard second-order center difference approximation. With nonuniform group widths, our treatments for Γ^{β}_{FP} and Γ^{γ}_{FP} are not equivalent to any standard finite difference approximation.

The definitions that we have given for σ^e can be meaningless for the first and last groups because a particle in the first group cannot upscatter and a particle in the last one cannot downscatter. Hence, we simply define $\sigma^{\gamma} = 0$ for the first and last groups, $\sigma^{\beta} = 0$ for the first group if $\beta(E_1) < 0$, and $\sigma^{\beta} = 0$ for the last group if $\beta(E_{NG}) > 0$. In energy deposition calculations, one is not interested in following particles down to thermal energies but rather only to energies sufficiently low that their residual range is small relative to the dimensions of the problem geometry. Particles slowing down below the cutoff energy are generally considered to deposit their remaining energy on the spot. This approach can be taken in the S_n calculation by setting the lower endpoint energy for the last group equal to the cutoff energy and defining an absorption cross section that has the effect of removing particles from the last group to thermal energies. We obtain a value for the absorption cross section by assuming the existence of a fictitious group below the last one. The width of this group is arbitrary, but we generally choose it to be the same as that which would be used for an additional real group. Denoting the midpoint energy of the fictitious group by E_f, the effective absorption cross section is found directly from Eq. (42):

$$\sigma_a^* = \frac{\beta(E_{NG})}{E_{NG} - E_f} \ . \quad (52)$$

In the computations section, it is shown that this absorption cross section is particularly useful in charge as well as energy deposition calculations.

Having defined the multigroup coefficients for σ^e, we now consider the validity of the truncated delta-function expansion, which must be used in conjunction with the transfer coefficients for σ^e. With delta-function scattering, the scattering source is equal to the angular flux:

$$S(\mu) = \int_0^{2\pi}\int_{-1}^{+1}\frac{1}{2\pi}\delta(\mu_0 - 1)\psi(\mu')d\mu'd\phi' = \psi(\mu) \ . \quad (53)$$

Thus, in an S_n calculation with delta-function scattering, the discrete scattering source should be equal to the discrete angular flux. Using a truncated delta-function expansion of degree $(N-1)$ in conjunction with a Gaussian quadrature set of order N, the S_n scattering source can be expressed as

$$S(\mu_i) = \sum_{l=0}^{N-1}\frac{2l+1}{4\pi}\sigma_l\phi_l P_l(\mu_i) \ , \quad i = 1, N \quad (54a)$$

where $\sigma_l = 1$ and

$$\phi_l = \sum_{k=1}^{N}\psi(\mu_k)P_l(\mu_k)w_k \ , \quad l = 0 \ , \quad N-1 \ . \quad (54b)$$

Let $\psi_p(\mu)$ be the unique polynomial of degree $(N-1)$ that interpolates the discrete angular flux values. The flux moments of ψ_p are given by

$$\phi_l^p = 2\pi\int_{-1}^{+1}\psi_p(\mu')P_l(\mu')d\mu' \ , \quad l = 0 \ , \quad N-1 \ . \quad (55)$$

Because the integrand is a polynomial of degree $(2N-1)$ or less, the integral can be exactly evaluated using the Gauss quadrature formula:

$$\phi_l^p = \sum_{k=1}^{N}\psi(\mu_k)P_l(\mu_k)w_k \ , \quad l = 0 \ , \quad N-1 \ . \quad (56)$$

Inspection of Eqs. (54b) and (56) shows that the S_n flux moments are identical to the flux moments of the interpolatory polynomial. Equation (54a) is then clearly seen to be the Legendre expression for the interpolatory polynomial. This gives the desired result:

$$S(\mu_i) = \psi(\mu_i) \ , \quad i = 1, N \ . \quad (57)$$

Thus, if cross-section expansions of degree $(N-1)$ are used in conjunction with Gauss quadrature sets of order N, our S_n representation for the Γ^{β}_{FP} and Γ^{γ}_{FP} terms will correctly cause particles to redistribute in energy without directional change. If other expansion orders or quadrature sets are used, the correct results cannot be guaranteed. Hence, it is *necessary*

that expansions of degree $(N - 1)$ be used in conjunction with Gauss quadrature sets of order N. It is important to recall that the use of such expansions and quadrature sets makes our treatment for the Γ^{α}_{FP} term spherical-harmonic-equivalent. This clearly adds to the credibility of our method.

It was previously mentioned that our method is restricted to one-dimensional slab and spherical geometries. This restriction is due entirely to the delta-function scattering. One-dimensional cylindrical geometry problems are really two-dimensional in direction space and there exists no two-dimensional quadrature sets of sufficient accuracy to treat delta-function scattering. In a future paper, we will present a new method for calculating S_n scattering sources that always treats delta-function scattering properly.[18] This method employs Legendre cross-section expansion coefficients to describe the scattering and it is algebraically equivalent to the standard S_n method for calculating scattering sources. It is significant to note that an option for the method will be available in the forthcoming ONEDANT code.[19] This code will be able to perform both Boltzmann and Fokker-Planck calculations in all three geometries.

In concluding this section, we wish to point out that Fokker-Planck solutions generally converge to Boltzmann solutions in an asymptotic fashion. That is to say, for any particular problem there usually exists a specific approximation order for which optimum results are obtained. Use of either higher or lower order approximations yields poorer agreement between the Fokker-Planck and Boltzmann solutions. Within this context, it is appropriate to note that the second-order Γ^{γ}_{FP} term introduces upscatter into calculations whether or not upscatter is present in the Boltzmann scattering kernel. This would suggest that it might not always be advantageous to include the Γ^{γ}_{FP} term if upscatter is not present. The computational cost of treating upscatter can be quite high in S_n calculations because of the need for outer iterations. We therefore suggest that the use of the Γ^{γ}_{FP} term be carefully considered in problems without upscatter.

COMPUTATIONAL RESULTS

In this section we provide computational results to demonstrate the effectiveness of our technique. Energy and charge deposition calculations have been performed for 1-MeV electrons isotropically incident upon slabs of cold (room temperature) aluminum. The slab thicknesses were 31.8×10^{-2} mm (12.5 mil; approximately one-sixth range), 63.5×10^{-2} mm (25 mil; approximately one-third range), and 127×10^{-2} mm (50 mil; approximate two-thirds range), respectively, designated as problems 1, 2, and 3. All calculations were performed with the ONETRAN code using a Gaussian S_8 quadrature set in conjunction with P_7 cross-section expansions. All sources were normalized to unity. Fifty energy groups of uniform width (ΔE = 18.37 keV) were used having maximum and minimum midpoint energies of 1.0 and 0.1 MeV, respectively. Since there is no upscatter at the energies of interest, the first-order continuous slowing down approximation ($\Gamma^{\gamma}_{FP} \equiv 0$) was used rather than the full second-order treatment. The "fictitious group" procedure was employed to obtain an effective absorption cross section for the last group [see Eq. (52)]. The width of the fictitious group was chosen to be the same as the width of the real groups.

The energy deposited in the k'th zone can be expressed as

$$D_e(r_k) = \left[\sum_{g=1}^{NG-1} \phi_g(r_k)\beta(E_g) + \phi_{NG}(r_k)\sigma_a^* E_{NG} \right] V_k \ , \tag{58}$$

where $\phi_g(r_k)$ denotes the scalar flux for group g in zone k and V_k is the zone volume. Note that the multigroup stopping power for the last group is equal to $\sigma_a^* E_{NG}$ rather than $\beta(E_{NG})$. This is a direct result of the fictitious group treatment. A particle slowing down into the fictitious group is actually "absorbed" by the medium and thus deposits all of its energy at the point of absorption. This causes the multigroup stopping power to be greater than the true stopping power:

$$\sigma_a^* E_{NG} = \beta(E_{NG})E_{NG}/(E_{NG} - E_f) > \beta(E_{NG}) \ . \tag{59}$$

This does not introduce significant error into the calculation as long as the number of particles actually escaping the system at energies lower than the cutoff energy is negligible.

The charge deposited in the k'th zone can be expressed as

$$D_c(r_k) = \phi_{NG}(r_k)\sigma_a^* V_k \ . \tag{60}$$

Only the last group contributes to the charge deposition because it is the only group in which particles can be absorbed.

It is significant to note that both the energy and charge deposition profiles can be obtained with the standard edit options available in ONETRAN. In the case of the energy deposition profile, it is necessary to include the stopping-power value for each group as an additional cross-section value at the top of the cross-section table.

[18] J. E. MOREL, "A Hybrid Collocation-Galerkin-S_N Method for Solving the One-Dimensional Neutron Transport Equation," to be submitted to *Nucl. Sci. Eng.*

[19] R. DOUGLAS O'DELL, FORREST W. BRINKLEY, Jr., and DUANE R. MARR, "Users' Manual for ONEDANT: A Code Package for One-Dimensional, Diffusion-Accelerated, Neutral-Particle Transport," Los Alamos National Laboratory report (to be published).

It is well known that the S_n equations conserve particles.[15] It follows that charge must also be conserved in our calculations simply because each particle carries a fixed amount of charge. It is not difficult to show that energy is also conserved in S_N calculations as long as the multigroup stopping powers [see Eq. (44b)] are used in calculating the energy deposited in the system. In particular, if the S_N equations for each group are multiplied by the corresponding midpoint group energy and summed (integrated) over all directions, groups, and zones, the following expression is obtained:

$$\sum_{g=1}^{NG} L_g E_g + \sum_{g=1}^{NG}\sum_{k=1}^{NZ} \phi_g(r_k)(\sigma_g^a E_g + \beta_g)V_k = \sum_{g=1}^{NG} Q_g E_g \ , \tag{61}$$

where

L_g = group particle leakage

NZ = total number of spatial zones

β_g = multigroup stopping power given in Eq. (44b)

Q_g = total group particle source.

Equation (61) states that energy is conserved, i.e.,

Energy escaped + energy absorbed = energy source.

Since the multigroup stopping powers, which are equal to the true stopping powers for all but the last group, are used in Eq. (58), it follows that energy is conserved in our calculations.

To obtain accurate solutions for comparison with our S_N calculation, we performed identical calculations using the coupled electron-photon Monte Carlo code,[20] TIGER. This code had to be modified to solve the Fokker-Planck equation rather than the coupled electron-photon Boltzmann equation. The necessary modifications were straightforward and will not be discussed here. The Monte Carlo solutions can be considered to be exact to within the inherent statistical error associated with Monte Carlo calculations. The number of particle histories generated in each calculation was chosen to be sufficiently large so that the maximum relative standard deviation of the energy deposited in any spatial zone was <2%.

Momentum transfer values were obtained by assuming Rutherford scattering[21] with Moliere[22] screening. The following expression results:

$$\alpha(E) = 2\pi Z(Z+1)(N_a r_0^2/A)(E+1)^2 E^{-2}(E+2)^{-2} \times [\ln(1+\eta^{-1}) - (1+\eta)^{-1}] \ , \tag{62}$$

where

E = electron kinetic energy in mc^2 (electron rest-mass) units

Z = atomic number of material

A = atomic weight of material

N_a = Avogadro's number

$r_0 = e^2/mc^2$ (classical electron radius)

$$\eta = 0.25\{Z^{1/3}/[0.885(137)]\}^2 E^{-1}(E+2)^{-1} \times [1.13 + 3.76(Z/137)^2(E+1)^2 E^{-1}(E+2)^{-1}].$$

The term $Z(Z+1)$ appears rather than Z^2 to approximately account for electron-electron deflections. The expression given by Rohrlich and Carlson[23] was used to obtain stopping power values:

$$\beta(E) = 2\pi r_0^2 N_a (Z/A)(E+1)^2 E^{-1}(E+2)^{-1} \times \{\ln[E^2(E+2)/(2I_0^2)] + f\}$$

and

$$f = 1 - [E(E+2)/(E+1)^2] - [(2E+1)/(E+1)^2]\ln 2 + E^2(E+1)^{-2}/8 \ , \tag{63}$$

where the electron kinetic energy is given in mc^2 units and I_0 is the mean ionization potential.

The discrete ordinates and Monte Carlo energy deposition profiles for problems 1, 2, and 3 are plotted in Figs. 2, 3, and 4, respectively. In addition, bulk energy deposition (total energy deposited in the slab) data are compared in Table I. Excellent agreement is obtained between the discrete ordinates and

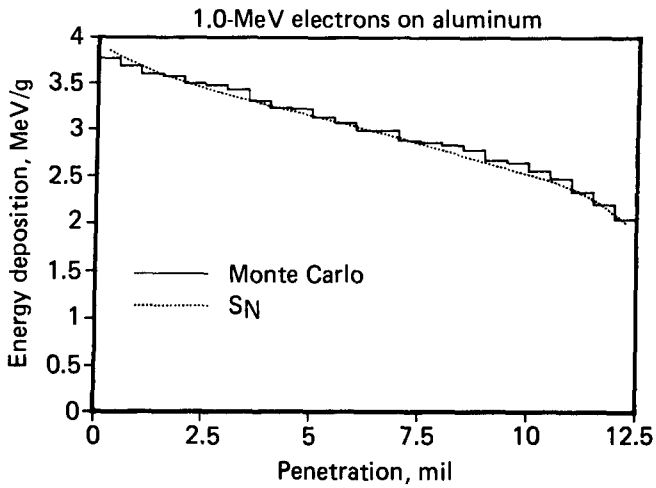

Fig. 2. Energy deposition profile comparision for problem 1.

[20] J. A. HALBLEIB and W. H. VANDEVENDER, *Nucl. Sci. Eng.*, **57**, 94 (1975).

[21] L. V. SPENCER, *Phys. Rev.*, **98**, 1597 (1955).

[22] G. MOLIERE, *Z. Naturforsch*, **2A**, 133 (1947).

[23] F. ROHRLICH and B. C. CARLSON, *Phys. Rev.*, **93**, 38 (1954).

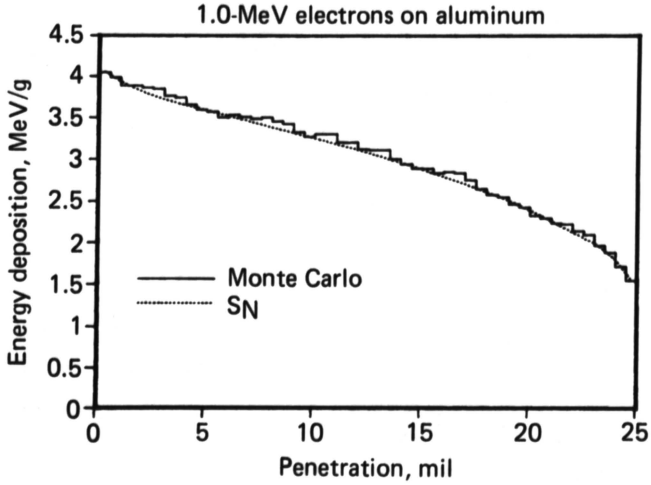

Fig. 3. Energy deposition profile comparison for problem 2.

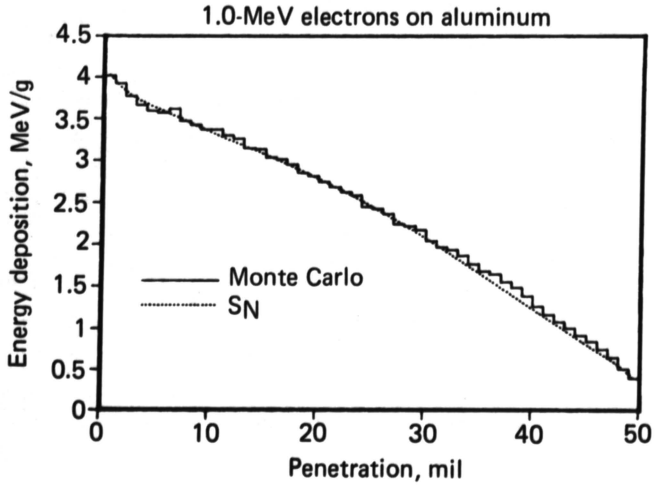

Fig. 4. Energy deposition profile comparison for problem 3.

Monte Carlo solutions in all cases. Comparisons of charge deposition profiles and bulk charge deposition data are similarly given in Figs. 5, 6, and 7 and Table II, respectively. The profiles clearly show that charge deposition calculations are subject to significantly more statistical error per analog particle history than energy deposition calculations. This is simply due to the fact that an electron can deposit energy throughout its suprathermal lifetime, but charge is deposited only at the point where the electron becomes thermalized. The Monte Carlo charge deposition profile for problem 1 is completely overwhelmed by statistical error and is essentially meaningless, but the bulk deposition value is quite good. Very good agreement is obtained in problems 2 and 3, but for problem 1 the discrete ordinates

TABLE I

Bulk Energy Deposition (MeV)

	Discrete Ordinates	Monte Carlo
Problem 1	0.255	0.258 ± 1%
Problem 2	0.512	0.518 ± ½%
Problem 3	0.795	0.806 ± ½%

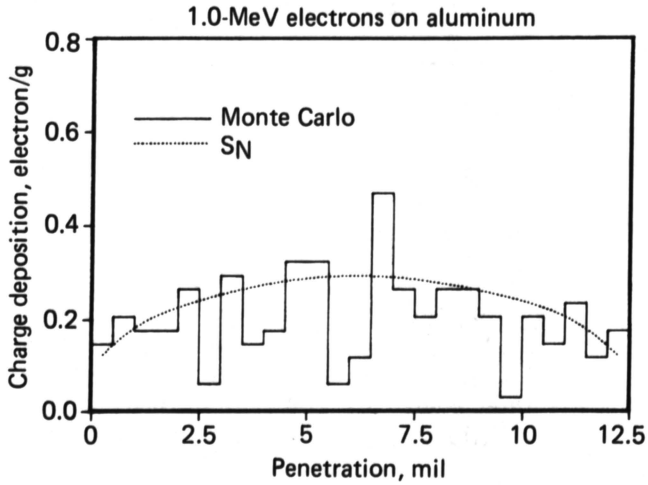

Fig. 5. Charge deposition profile comparison for problem 1.

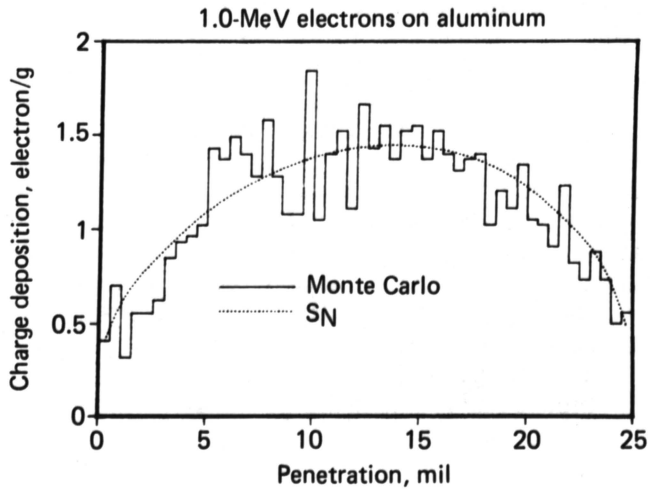

Fig. 6. Charge deposition profile comparison for problem 2.

value for the bulk deposition is ~18% greater than the Monte Carlo value. The agreement is distinctly poorer for this datum than it is for the others. Further data comparisons suggest an explanation for this.

The differential reflected and transmitted current

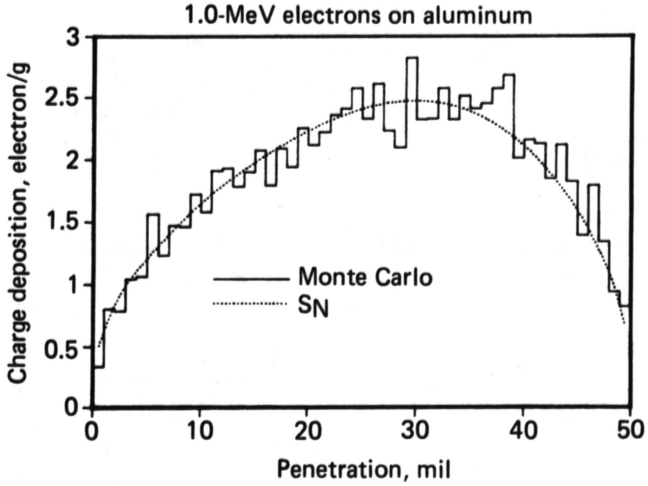

Fig. 7. Charge deposition profile comparison for problem 3.

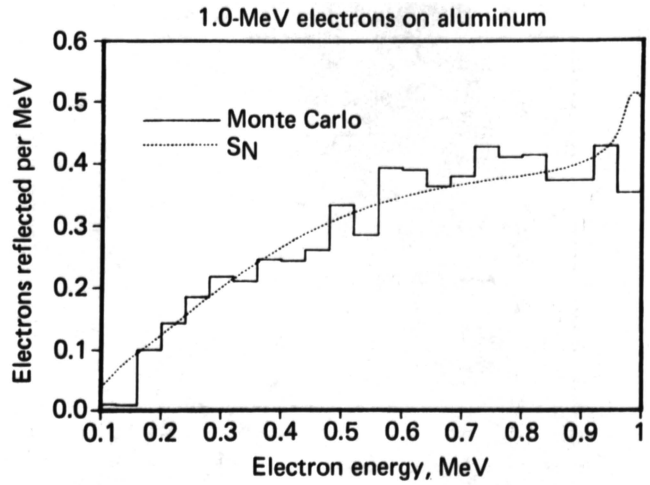

Fig. 8. Reflected current spectrum comparison for problem 2.

spectra for problem 2 are plotted in Figs. 8 and 9, respectively. The reflected spectra show good agreement except near the source energy where the discrete ordinates solution becomes more peaked than the Monte Carlo solution. The transmitted spectra are clearly in serious disagreement. The peak in the discrete ordinates spectrum appears to be properly centered, but the spectrum is much too broad. The spectral agreement is good only at the lowest energies. Such low energy agreement is necessary to account for the good charge deposition profile agreement. Although it is not obvious from the plot, the zeroth and first moments of the spectrum (i.e., the total number of particles and the total amount of energy being transmitted, respectively) are essentially correct. This is necessary to account for the good energy deposition profile agreement.

The fact that the reflected spectra are in good agreement while the transmitted spectra are not suggests that the broadening effect may generally be more pronounced at larger distances from the source than at smaller distances. Comparisons of the internal flux spectra (not shown) confirm this notion. The broadening is essentially nonexistent in the first

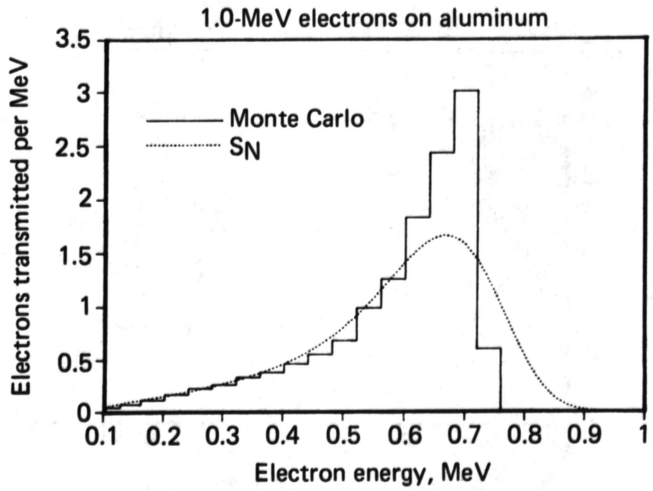

Fig. 9. Transmitted current spectrum comparison for problem 2.

TABLE II

Bulk Charge Electron Deposition

	Discrete Ordinates	Monte Carlo
Problem 1	0.020	0.017 ± 3%
Problem 2	0.198	0.193 ± 1%
Problem 3	0.643	0.651 ± 1%

(left) zone, but it steadily increases with increasing distance from the source.

The observed spectral broadening can be explained in terms of an excess of energy-loss straggling in the calculations. Because there is no energy-loss straggling under the continuous slowing down approximation; any energy-loss straggling present in the discrete ordinates calculations is excessive. Although straggling effects must decrease with decreasing group width, it is clear that some straggling is always present under our multigroup approximation. This inherent energy-loss straggling is the source of all the discrepancies between the discrete ordinates and Monte Carlo solutions. For instance, let us consider its effect on charge deposition. Under the continuous slowing down approximation, an electron thermalizes (and thereby deposits its charge) only after it has traveled

a cumulative pathlength equal to its associated range. However, under our multigroup approximation, it is possible for an electron to undergo a sufficient number of collisions to thermalize over any pathlength. Of course, as the group width decreases, the probability that an electron will thermalize after traveling a distance exactly equal to a range approaches unity, but with any nonzero group width, there is some characteristic pathlength interval over which the charge deposition (or equivalently the electron range) is effectively smeared. This effect is referred to as range straggling. As the slab thickness is decreased, range straggling must eventually cause the charge deposition to be overestimated. We believe that the reduced level of agreement obtained for the bulk charge deposition in problem 1 is due to the onset of this effect. The slab is clearly thin with respect to charge deposition since only ~1.7% of the incident charge is deposited.

It is important to note that straggling is not unique to the multigroup approximation. It is also obtained with finite difference approximations. This follows from the conditional equivalence of our multigroup method to standard finite difference schemes. It is also important to note that this equivalence suggests an alternate but equally valid interpretation of the observed discrete ordinates deficiencies. In the regions where the straggling effects are most severe, the spectral derivatives are large and rapidly varying in the high energy region of the peak. A first-order difference scheme cannot be expected to adequately represent such derivatives unless the energy mesh (group width) is exceedingly fine. Since our treatment for the Γ^{β}_{FP} term is always first-order accurate, we are lead to the important conclusion that spectral solutions can be expected to rapidly converge with decreasing group width only in problems with spectra that vary slowly as a function of energy.

To gain some insight into the convergence properties of the solutions as a function of group width, additional calculations for problem 2 were performed using 25 and 100 energy groups of uniform width, respectively. The corresponding energy deposition profiles and transmitted current spectra are compared in Figs. 10 and 11, respectively. The 25-group energy deposition profile is completely converged, but the transmitted current spectrum remains in considerable error even with 100 groups. The spectral convergence rate is obviously quite slow. It would appear that over 700 groups are necessary to achieve convergence.

The rapid convergence rate of the energy deposition profile is indicative of a generally rapid convergence rate for all scalar quantities. However, we wish to stress that poor spectral convergence occurs only in problems having spectra that change rapidly as a function of energy.

It is informative to note that the 25-, 50-, and 100-group calculations required ~17.4, 24.2, and

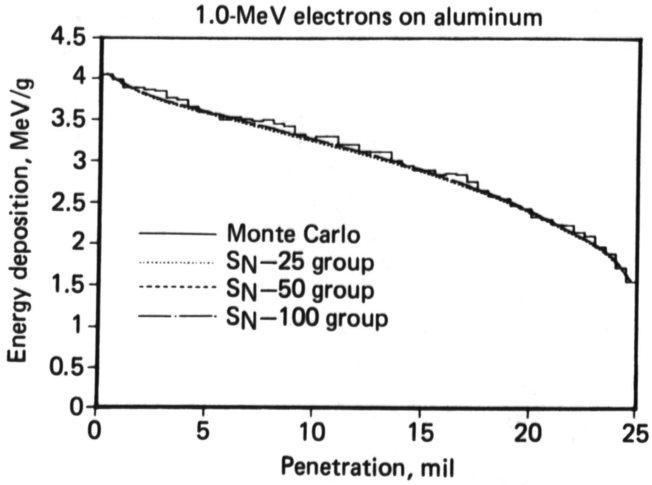

Fig. 10. Energy deposition profile comparison with various group structures for problem 2.

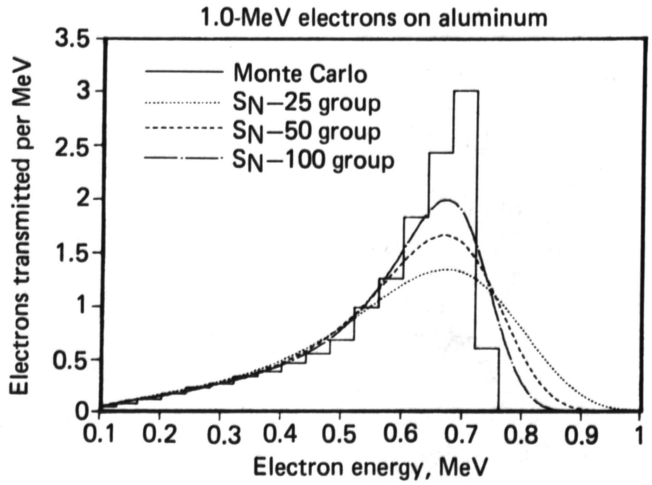

Fig. 11. Transmitted current spectrum comparison with various group structures for problem 2.

38.3 s, respectively, of central processor unit time to execute on a CDC-7600 computer. Under normal circumstances, one would expect the execution times to scale linearly with the number of groups. However, it is clear that the execution time per group decreases as the total number of groups is increased. In particular, the average number of inner iterations performed per group decreases. It is well known that the inner iterations required to converge in any S_N calculation decrease as the dominance ratio (σ_s/σ_t) approaches zero. For the specific problems under discussion, the dominance ratio for group g can be expressed as

$$\sigma_s/\sigma_t = \frac{\alpha(E_g)N(N-1)/2}{\alpha(E_g)N(N-1)/2 + \beta(E_g)/(E_g - E_{g+1})} . \quad (64)$$

With a fixed quadrature order, the dominance ratio clearly decreases as the group width is decreased. This explains the observed behavior. It is significant to note that with a fixed group structure, the dominance ratio increases as the quadrature order is increased. Thus, if the inner iteration convergence rate is poor due to a large quadrature order, it can be improved by increasing the number of groups in such a way that the associated group widths are reduced. Although Eq. (64) is quantitatively specific to a restricted class of problems, it is qualitatively correct for all cases. That is to say that the dominance ratio always increases with increasing quadrature order and decreases with decreasing group width.

To test our multigroup approximation to the second-order operator, Γ^{γ}_{FP}, we have performed a calculation of the relaxation of an initially non-Maxwellian alpha-particle distribution within a spatially infinite background plasma composed of deuterium and tritium at a temperature of 50 keV. The general form of the Fokker-Planck equation that describes such a process is

$$\frac{1}{v}\frac{\partial}{\partial t}\phi(t,E) - \Gamma^{\beta}_{FP}\phi(t,E) - \Gamma^{\gamma}_{FP}\phi(t,E) = 0 \ , \qquad (65)$$

where v is the particle velocity, and $\phi(t,E)$ is the particle flux differential in energy. The particle density, $N(t,E)$, is related to the flux by

$$N(t,E) = \frac{1}{v}\phi(t,E) \ . \qquad (66)$$

Equation (65) was solved with the time-dependent discrete ordinates neutron transport code, TIMEX. An infinite medium solution was obtained by employing a single spatial zone in slab geometry with a reflective boundary condition at each face. A Gaussian S_2 quadrature set was used in conjunction with 50 energy groups. The groups were of uniform width and spanned the energy range from 200 to 0 keV. The fictitious group procedure is inappropriate for such a group structure. Therefore, the previously described alternative procedure was employed whereby σ^{γ} is set to zero for both the first and last group. It was not necessary to set σ^{β} to zero for either the first or last group because the stopping power is positive for the first group and negative for the last one.

Appropriate expressions for the stopping power and mean-square stopping power were derived from the Fokker-Planck functions given by Melhorn and Duderstadt[10] using a rather complicated coordinate transformation that we do not give here. The contribution to the stopping power from the i'th ion component of the plasma is given in units of keV/cm by

$$\beta_i(E) = 1.303 \times 10^{-19} Z^2 Z_i^2 A N_i \Lambda_i/(A_i E) \times [\mathrm{ERF}(\epsilon_i) - (2\epsilon_i/\sqrt{\pi})\exp(-\epsilon_i^2)(1 + A_i/A)] \ , \qquad (67)$$

where

$\mathrm{ERF}(x)$ = error function

$\epsilon_i^2 = (A_i/A)(E/kT_i)$

Z = atomic number of transport particle

A = atomic weight of transport particle

N_i = number density (number/cm^3) of plasma ion component

E = energy of transport particle in keV

kT_i = temperature of plasma ion component in keV.

An expression for the Λ_i term in Eq. (67) is given by Antal and Lee[8]:

$$\Lambda_i = \Lambda_i^* = 35.72 + \ln[A_i\sqrt{A}/(A + A_i)] + \frac{1}{2}(EkT_e/N_e) \ , \quad E/E^* \geqslant 1 \ ,$$

$$= \Lambda_i^* + \frac{1}{2}\ln(E/E^*) \ , \quad E/E^* < 1 \ , \qquad (68a)$$

where kT_e is the electron temperature in keV, N_e is the electron number density (number/cm^3) and

$$E/E^* = [(137/2)ZZ_i(c/v)]^2 \ , \qquad (68b)$$

where c/v is the ratio of the speed of light to the speed of the transport particle. The plasma electron contribution to the stopping power is given by

$$\beta_e(E) = 2.375 \times 10^{-16} Z^2 A N_e \Lambda_e / E[\mathrm{ERF}(\epsilon_e) - (2\epsilon_e/\sqrt{\pi})\exp(-\epsilon_e^2) \times (1 + 5.485 \times 10^{-4}/A)] \ , \qquad (69)$$

where

$$\epsilon_e^2 = (5.486 \times 10^{-4}/A)(E/kT_e)$$

$$\Lambda_e = \Lambda_e^* = 32.17 + \ln(kT_e/\sqrt{N_e}) \ , \quad kT_e \geqslant kT_e^*$$

$$= \Lambda_e^* + \frac{1}{2}\ln(kT_e/kT_e^*) \ , \quad kT_e < kT_e^*$$

$$kT_e^* = 3.628 \times 10^{-2} Z^2 \ (\mathrm{keV}) \ .$$

The contribution to the mean-square stopping power from the i'th ion plasma component and the electron component are respectively given in units of (keV)^2/cm by

$$\gamma_i(E) = 2.605 \times 10^{-19} Z^2 Z_i^2 A N_i \Lambda_i kT_i / (A_i E)[\mathrm{ERF}(\epsilon_i) - (2\epsilon_i/\sqrt{\pi})\exp(-\epsilon_i^2)] \ , \qquad (70)$$

and

$$\gamma_e(E) = 4.749 \times 10^{-16} Z^2 A N_e \Lambda_e k T_e / E[\mathrm{ERF}(\epsilon_e) - (2\epsilon_e/\sqrt{\pi}) \exp(-\epsilon_e^2)] \quad . \tag{71}$$

Although the momentum transfer was assumed to be zero in the calculation, for the sake of completeness we include the appropriate respective expressions for the plasma ion and electron contributions to the momentum transfer in units of (cm^{-1}):

$$\alpha_i(E) = 6.514 \times 10^{-20} Z^2 Z_i^2 N_i \Lambda_i / E^2 \{\mathrm{ERF}(\epsilon_i)[1 - (2\epsilon_i^2)^{-1}] + \exp(-\epsilon_i^2)/(\epsilon_i \sqrt{\pi})\} \tag{72}$$

and

$$\alpha_e(E) = 6.514 \times 10^{-20} Z^2 N_e \Lambda_e / E^2 \{\mathrm{ERF}(\epsilon_e)[1 - (2\epsilon_e^2)^{-1}] + \exp(-\epsilon_e^2)/(\epsilon_e \sqrt{\pi})\} . \tag{73}$$

For simplicity a composite ion component with $Z = 1.0$ and $A = 2.5$ was used to represent the deuterium and tritium components, and the plasma density was assumed to be 0.2125 g/cm^3. The calculation was begun with a uniform flux distribution, i.e.,

$$\phi(0, E_g) = \phi_0 \quad , \quad g = 1, 50 \quad . \tag{74}$$

The constant ϕ_0 was chosen to achieve a unit integral density:

$$\sum_{g=1}^{50} \phi(E_g)/v_g = 1.0 \quad . \tag{75}$$

The calculation was carried out to a sufficiently late time so as to obtain the equilibrium solution. It is well known that the equilibrium solution to the Fokker-Planck equation for a problem of this type is the Maxwellian distribution corresponding to the background plasma temperature, T:

$$N(E) = N_0 2\sqrt{E} \exp(-E/kT)/\sqrt{\pi}(kT)^{3/2} \quad . \tag{76}$$

The discrete ordinates and exact equilibrium solutions are compared in Fig. 12. The agreement obtained between the two solutions is very good for all but the first and last groups. It is obvious that the first group (highest energy) has far too many particles. However, it is important to realize that setting σ^γ to zero for that group causes all particles that would normally scatter to higher energies to remain in that group. Since there is actually a significant number of particles at energies >200 keV, one would expect the first group to have too many particles. However, it is rather surprising that the overpopulation of the first group does not significantly perturb the population in neighboring groups. Although it is clearly desirable, we are uncertain as to whether such behavior can be expected in general. In any event, the best course of action is to structure the energy groups so they span a sufficiently large energy range, making the number of particles in the first group negligibly small. The last group is also overpopulated, although to a much lesser extent than the first group. The overpopulation of the last group does seem to have caused the next several groups to be slightly underpopulated, but this perturbation of the populations seems to be almost uniformly distributed among the neighboring groups rather than being most severe in the nearest groups. We can offer no explanation for this behavior. However, the fact that the derivative of the exact solution becomes unbounded in the limit as $E \to 0$ suggests that the error associated with the last group is due simply to a lack of resolution. Over all, we feel that the results obtained in this calculation demonstrate that our multigroup treatment of the Γ_{FP}^{γ} operator is a valid one.

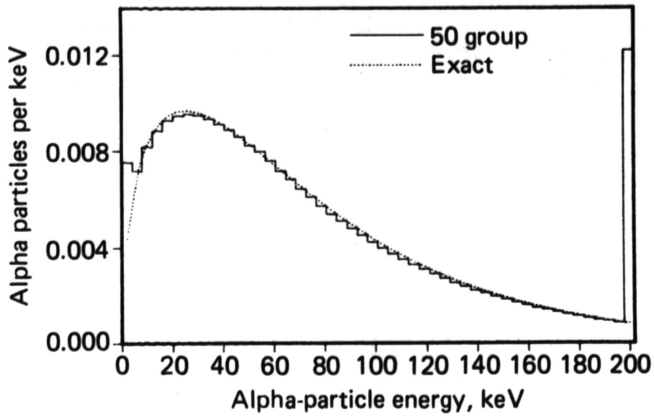

Fig. 12. Equilibrium density comparison for alpha particles relaxing in a 50-keV deuterium-tritium plasma.

CONCLUSIONS AND RECOMMENDATIONS

The results of this work are briefly summarized as follows:

1. A method has been developed for performing Fokker-Planck calculations in one-dimensional slab and spherical geometries using standard (unmodified) discrete ordinates neutron transport codes. A new discrete ordinates code called ONEDANT, which allows Fokker-Planck calculations to be performed in one-dimensional cylindrical geometry as well, will soon be available.

2. Solutions for energy- and angle-integrated quantities such as energy and charge deposition can be accurately and efficiently calculated for electrons using our method.

3. Differential energy spectra may sometimes require an inordinately large number of energy groups to be accurately calculated. This occurs only in problems having spectra that rapidly change as a function

of energy. Such spectra generally appear only in problems having significantly large (with respect to the particle range) sourceless regions.

4. Our treatment for the angular operator, Γ^{α}_{FP} [see Eq. (11a)], is equivalent to a spherical-harmonic approximation. Therefore, accurate values can be expected for the angular flux moments, but the angular flux itself may be negative along certain quadrature directions.

5. Our treatment for the energy operator, Γ^{e}_{FP} [see Eq. (11b)], is a multigroup method that is sometimes equivalent (depending on the group structure) to a standard finite-difference treatment. Particle energy and charge are always conserved.

6. The dominance ratio, σ_s/σ_t, for each group approaches unity with increasing quadrature order and approaches zero with decreasing group width.

From these results we conclude that our method for solving the Fokker-Planck equation represents a valuable alternative to existing methods. Clearly the most significant advantage of the method is that it allows widely available discrete ordinates neutron transport codes to be directly utilized for Fokker-Planck calculations. Many additional calculations will have to be made in the future to fully document the accuracy and applicability of the method, but the computational results that have been presented give a fairly clear picture of what can be expected. The spectral convergence problem represents the most obvious deficiency of the method. However, we strongly suspect that any other method will give a similarly poor convergence rate if it utilizes a first-order treatment for the Γ^{β}_{FP} term. One possible solution might be to develop a high order finite-element treatment that would be compatible with existing discrete ordinates codes. This should be investigated in the future. The fact that the dominance ratio approaches unity with increasing quadrature order could mean reduced efficiency in calculations requiring high quadrature orders (e.g., problems with normally incident sources). However, it should be noted that the ONEDANT code will not only allow Fokker-Planck calculations in cylindrical geometry, but will also perform diffusion-synthetic convergence acceleration[24] of the inner iterations. Theoretical considerations suggest that this technique might be very effective in accelerating the convergence of Fokker-Planck calculations. When ONEDANT becomes available, we intend to investigate its effectiveness. We also intend to investigate the accuracy of our method in cylindrical geometry calculations.

Because the three-dimensional Monte Carlo neutron transport code,[25] MORSE, uses the same cross-section data that discrete ordinates codes use, the question naturally arises as to whether Fokker-Planck calculations could be performed with this code. At the present time, the answer is no. The algorithm currently used in MORSE to sample scattering angles cannot treat the delta-function scattering that arises from the Γ^{e}_{FP} term. However, it is conceivable that a new general purpose algorithm could be developed for MORSE that would properly treat such scattering. This would result in a unique and powerful capability for three-dimensional forward or adjoint Fokker-Planck calculations.

ACKNOWLEDGMENTS

The author wishes to acknowledge many invaluable discussions about the Fokker-Planck equation with T. A. Mehlhorn of Sandia National Laboratories.

Sandia National Laboratories is a U.S. Department of Energy (DOE) facility. This work was supported under contract by DOE.

---

[24]R. E. ALCOUFFE, *Nucl. Sci. Eng.*, **64**, 374 (1977).

[25]M. B. EMMETT, "The MORSE Monte Carlo Radiation Transport Code System," ORNL-4972, Oak Ridge National Laboratory (1975).